Desalination and Water Treatment
www.deswater.com

doi: 10.5004/dwt.2019.23327

138 (2019) 173–182
January

Application of CuO/AC in DBD plasma for dye wastewater treatment: synthesis, optimization, and coupling mechanism

Yongjun Shen*, Yunli Wang, Kaixia Fan

School of Chemistry and Chemical Engineering, Nantong University, Nantong, 226019, China, emails: shenyj@ntu.edu.cn (Y. Shen), 17080004@ntu.edu.cn (Y. Wang), 1808320004@yjs.ntu.edu.cn (K. Fan)

Received 18 May 2018; Accepted 18 October 2018

ABSTRACT

Acid turquoise blue A (ATBA) is treated by the combined dielectric barrier discharge (DBD) plasma and AC supported CuO (CuO/AC). CuO/AC is prepared by incipient wetness impregnation method. X-ray diffraction, N_2 adsorption/desorption isotherm, and scanning electron microscope are used to characterize the CuO/AC. Interactive effects of initial pH, conductivity value, input power, and CuO/AC dosage on the decolorization rate of ATBA are investigated. The predicted decolorization rate of ATBA reaches to 97.12% under the optimal condition, only have 1.95% error compared with the experimental value (95.87%). The possible coupling mechanisms of combined DBD plasma and CuO/AC are proposed.

Keywords: Dielectric barrier discharge plasma; CuO/AC; Synthesis; Optimization; Coupling mechanism

1. Introduction

Several textile printing mills discharge bulky amount of organic effluents into the nearby aquatic streams without any appropriate effluent treatment. The dye molecules in wastewater have complex aromatic structure which makes it difficult to be biodegraded voluntarily. The toxic intermediate products can do harm to the environment even the human health [1–3]. Removing dye pollution from the industrial effluents has become an important issue.

As an eco-innovative and highly competitive technology, non-thermal plasma (NTP) has been widely applied on the research of materials [4–7], polluted gas [8,9], and soils [10,11] due to its chemical-free operation. When the high voltage is applied between two electrodes, electrical discharges are created and an environment with extra high physical and chemical activity is provided, thus generating highly energetic electrons and chemically reactive species including hydroxyl radical (·OH), hydrogen radical (·H), ozone (O_3), hydrogen peroxide (H_2O_2), etc. [11,12]. These active substances can effectively degrade organic pollutants without secondary pollution [13], hence NTP is increasingly investigated for wastewater treatment as an advanced oxidation process. Mercado-Cabrera et al. [14] studied the simultaneous degradation of phenol and m-cresol in one aqueous solution using DBD plasma, and the degradation efficiency of 99% was obtained. Zhang et al. [15] employed DBD plasma to degrade 2,4-dichlorophenol, the toxic effect of 2,4-dichlorophenol was obviously reduced, and the work demonstrated that DBD plasma was a feasible method for chlorophenol treatment in wastewater.

However, low energy efficiency and high energy consumption of DBD plasma limit the wide application of this technology. The combination of catalysts would be able to overcome this shortcoming [12]. Particularly, physical properties of a discharge can be affected and more active species will be formed, leading to the increase of collision probability between pollutant molecules and active substances, hence greatly save cost as well as improve biodegradation efficiency [16]. Copper (Cu) is a common and effective precursor in catalytic applications [17]. Some researchers found that activated carbon (AC) is a good support for copper, bimetallic

* Corresponding author.

copper or copper oxide [18,19], and is widely used in adsorption procedure due to its porous structure, high surface area, and excellent chemical stability [20–22]. Therefore, CuO/AC has drawn much attention as a promising catalyst for the removal of benzene and other gas pollutants in recent years. Ren et al. [23] found that CuO/AC can effectively remove PH_3 less than 1 mg/m^3, the purification efficiency was nearly 100% at 100°C with an oxygen volume fraction of 1.6%. He et al. [16] applied different MO_x/AC (M = Fe, Ag, Zn, Mn, and Cu) catalysis in NTP to remove benzene, and NTP coupled CuO/AC exhibited the highest benzene elimination capability, removal efficiency of 90.6% which was 40% more than NTP alone was obtained at energy density of 70 J.L^{-1}.

The objective of the presented work was to investigate whether it can get better treatment efficiency when CuO/AC was applied in DBD plasma to treat dyeing wastewater. CuO/AC was frequently used to treat polluted gases and showed an excellent removal efficiency, but the applications of CuO/AC in wastewater treatment are relatively few. Furthermore, the process of combined DBD plasma and CuO/AC on wastewater treatment along with its coupling mechanism has hardly been studied by researchers. It was believed that the excellent catalytic effect and adsorption performance of CuO/AC can effectively improve the degradation efficiency of wastewater by DBD plasma. Moreover, the combination system can availably remove the odor of wastewater and the harmful gas formed during degradation process.

ATBA which is a common used dyestuff with complex structure is selected as model pollutant in this work. The process of combined DBD plasma and CuO/AC is adopted to treat ATBA. CuO/AC is prepared by incipient wetness impregnation method. X-ray diffraction (XRD), N_2 adsorption/desorption isotherm, and scanning electron microscope (SEM) techniques are used to characterize CuO/AC. The specific surface area is calculated using Brunauer–Emmett–Teller method, and the pore size distribution of mesopores is derived from the desorption branch of N_2 isotherm. As a statistical-based technique, the response surface methodology (RSM) is a powerful tool for experimental design compared with conventional multifactor experiments [24]. Fu et al. [25] agreed that RSM can be widely conducted to analyze the effects of multiple factors and their interaction. Therefore, RSM is used in this work to obtain the optimal condition, as well as to investigate the interactive effects of initial pH (*A*), conductivity value (*B*), input power (*C*), and CuO/AC dosage (*D*) on decolorization rate of ATBA. The synergistic effect of combined DBD plasma and CuO/AC system is also investigated, and the possible coupling mechanisms are proposed based on the results.

2. Experimental procedure

2.1. Materials

All the chemicals used in the experiment are of analytical grade. ATBA was purchased from Shanghai Jiaying Co., Ltd., China. Granulated coal-based AC was crushed to 0.25–0.40 mm (Shanghai Experiment Reagent Co., China). The conductivity value of solution was adjusted by KNO_3 (Aladdin Industrial Co., China). NaOH (Shantou Xilong Chemical Co., Ltd., China) or H_2SO_4 (Shanghai Chemical Co., Ltd., China) was used to adjust the pH value of solution.

2.2. Synthesis of CuO/AC

The CuO/AC was prepared by incipient wetness impregnation method. AC was washed with ultrapure water and dried at 105°C. 13.65 g $Cu(NO_3)_2{\cdot}3H_2O$ and 10 g AC were dissolved in 5 mL ultrapure water under constant stirring, then the mixture was kept at 60°C for 10 min and dried at room temperature for 8 h. An infrared lamp (100 W) was used to irradiate the mixture at 65°C for 6 h. Afterwards, the mixture was further dried at 150°C for 1 h (remove solvents and moisture) and 300°C for 4 h (remove nitrate ion). Subsequently, the product was screened by 200 mesh to remove free metal.

2.3. Characterization of CuO/AC

XRD patterns were recorded on D/MAX-IIIA X-ray diffractometer (Rigaku, Japan) at 40 kV and 80 mA. And Cu-K_α radiation (λ = 0.15406 nm) was used. The morphology of CuO/AC was characterized by S-3000N scanning electron microscopy (Hitachi, Japan) at an accelerating voltage of 20 kV. The N_2 adsorption/desorption isotherms of catalysts at 77 K were measured by ASAP 2460 instrument. The pore size distributions of mesopores were determined by Barrett–Joyner–Halenda (BJH) method [26].

2.4. Experimental design

The schematic of plasma-catalyst system is shown in Fig. 1. 10 mL ATBA solution (30 mg/L) with a certain amount of CuO/AC catalyst was treated in quartz reaction kettle (DBD-100B, Nanjing Suman Electronics Co., Ltd., China). The aluminum electrodes on both side of reaction kettle were in air, and it was a filamentary discharge. The input power of system was mutually regulated by a circumscribed voltage regulator and a plasma generator (CTP-2000K, Nanjing Suman Electronics Co., Ltd., China). After 150s reaction, the absorbance of ATBA solution was measured at 638 nm with Ultraviolet/Visible spectrophotometer (UV 752, Shanghai Sunny Hengping Scientific Instrument Co., Ltd., China). The decolorization rate of ATBA was calculated by Eq. (1)

$$Y = \frac{c_0 - c}{c_0} \times 100\% \tag{1}$$

where Y is the decolorization rate of ATBA (%), c is the residual concentration of ATBA after treatment (mg/L), and c_0 is the initial concentration of ATBA without treatment (mg/L).

Design-Expert 8.0 software was used for experimental design and data analysis. RSM based on Box–Behnken design (BBD) in software was employed to evaluate the effects of key variables. The experimental range and levels of independent variables are shown in Table 1. The relationship between dependent and independent variables is explained by a second-order model in the form of quadratic polynomial equation:

$$Y = \beta_0 + \sum \beta_i X_i + \sum \beta_{ii} X_i^2 + \sum \beta_{ij} X_i X_j \tag{2}$$

where Y predicts response of decolorization rate of ATBA, β_0 is a constant coefficient, β_i, β_{ii}, and β_{ij} are coefficients for

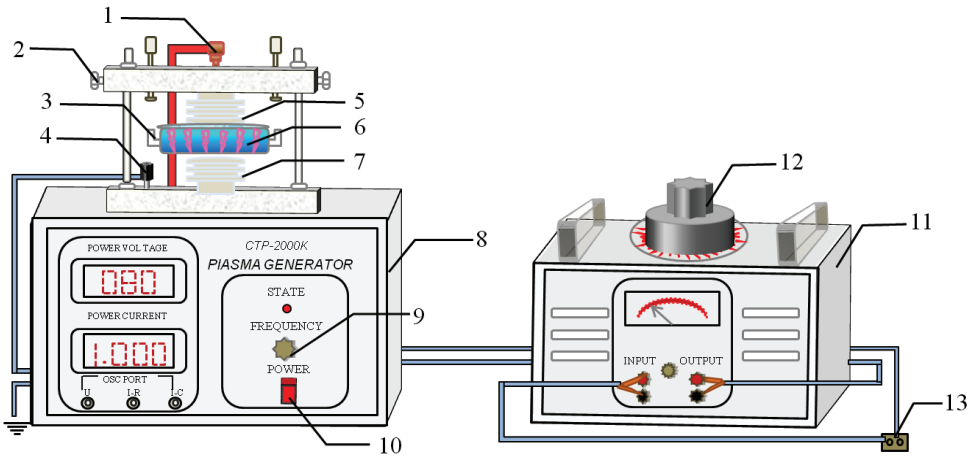

Fig. 1. Experimental setup. (1) High voltage connection bolt, (2) air gap adjusting screw, (3) reaction kettle, (4) earth pole connection bolt, (5) top electrode, (6) ATBA solution with CuO/AC, (7) lower electrode, (8) plasma generator, (9) current adjustment knob, (10) switch button, (11) voltage regulator, (12) regulation valve and (13) alternating current power source.

Table 1
Experimental range and levels of the independent variables

Factors	Parameter coding	Low level	High level
Initial pH	*A*	2	12
Conductivity value (μS/cm)	*B*	100	2,500
Input power (W)	*C*	63	105
CuO/AC dosage	*D*	0	0.04

linear, quadratic, and interaction factor effects, respectively. X_i and X_j represent the parameter value of each factor [27].

3. Results and discussion

3.1. Catalyst characterization

The XRD patterns are shown in Fig. 2. Characteristic reflections at 2θ = 32.5°, 35.5°, 38.7°, 48.7°, 53.4°, 58.3°, 61.5°, 66.2°, 68.1°, 72.4°, 75.2° correspond to CuO (JCPDS card No. 45-0937) with lattice constants of a = 4.685 nm, b = 3.426 nm, and c = 5.130 nm. There are no peaks of Cu_2O on the diffraction line. It suggests that Cu is loaded on the AC in the form of CuO after impregnation. The average size of CuO (D) is estimated to be about 86 nm by Scherrer's formula. The equation is as follows [28]:

$$D = \frac{K\lambda}{\beta\cos\theta} \tag{3}$$

where D is the average size of CuO, K is the shape factor, λ is the X-ray wavelength of Cu K_α radiation (0.15406 nm), θ is the Bragg angle and β is the line broadening at half the maximum intensity.

N_2 adsorption/desorption isotherms and pore size distributions of AC and CuO/AC are shown in Fig. 3. From

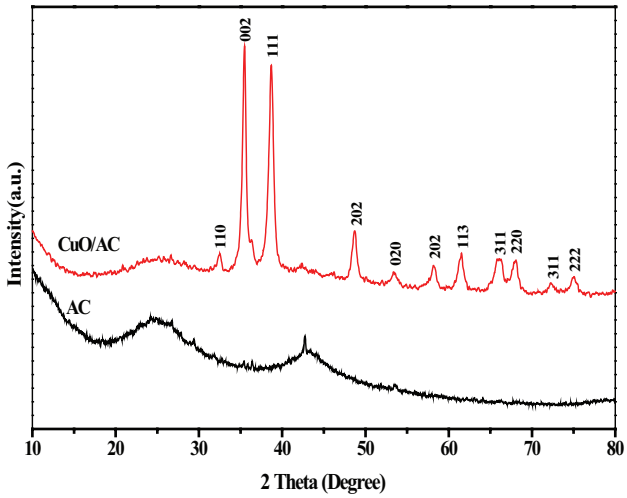

Fig. 2. XRD patterns of AC and CuO/AC.

Fig. 3(a), the adsorption plateaus for AC are systematically above those of CuO/AC, which indicates that the adsorption capacity of CuO/AC is relatively lower than that of AC. As could be seen from Fig. 3(b), the peak pore diameter is approximated to be ca. 3.8 nm. The calculated specific surface areas of AC and CuO/AC are 534 and 473 m^2/g, respectively. Compared with AC, the specific surface area of CuO/AC decreases by 11%, which is consistent with the test result of N_2 adsorption/desorption isotherms.

The SEM images of the AC and CuO/AC are shown in Fig. 4. SEM is regularly used for surface morphology and physical properties of catalyst [29]. It could be seen from Fig. 4(a) that AC has many holes which are composed of sheet-like nanoclusters. The result suggests that AC has a good load effect on metal oxides. Fig. 4(b) shows that the prepared CuO/AC catalyst still possesses a porous surface. Besides, feather-like CuO are dispersed evenly on the AC surface. Maybe the calcination or the impregnation of CuO results in the irregular shapes of CuO/AC.

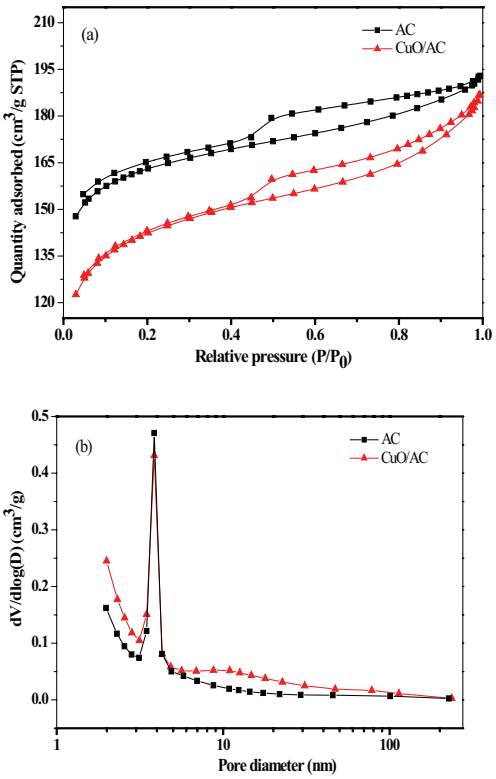

Fig. 3. (a) N_2 adsorption/desorption isotherms at 77 K of AC and CuO/AC and (b) BJH pore size distribution plots of AC and CuO/AC.

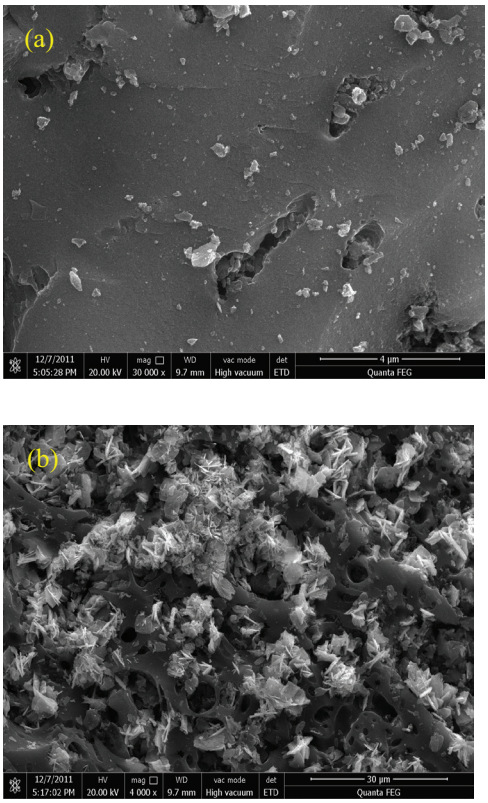

Fig. 4. SEM images. (a) AC and (b) CuO/AC.

3.2. Analysis on the degradation of ATBA by RSM

3.2.1. Establishment of model equation and significant analysis

According to the software design, the response surface experimental scheme is shown in Table 2. Table 3 shows the analysis of variance. From Table 3, the *p* value of model is far less than 0.0001 which shows that the experimental model has a remarkable adaptability. *p*-value of 'Lack of fit' is 0.4234 (>0.05), it illustrates that the nonlinear relationship between factors and response is significant, and the model is reliable. p-values of *A*, *C*, *D*, *AD*, C^2, and D^2 are less than 0.05, representing that the effects of those variables are obvious. The influence of variables on decolorization rate is determined by *F* value. Large *F* value means that the variable has a great influence on decolorization rate [30]. That said, the influence sequence of single factor on decolorization rate is $C > A > D > B$. For good measure, the perturbation plot for decolorization rate is shown in Fig. 5. The curvature of curve represents the sensitivity of each factor to response value [31], and it can be concluded that the decolorization rate is the most sensitive to input power (*C*), then initial pH (*A*), CuO/AC dosage (*D*), conductivity value (*B*), this is consistent with the result of *F* value. The determination coefficient (R^2) of model is 0.9224, the adjustment coefficient (R_{adj}^2) is 0.8501, and the difference between two coefficients is less than 0.2, indicating that the model has good precision and creditability. Through the fitting analysis of response surface system, regression equation for decolorization rate of ATBA (*Y*) is shown in Eq. (4):

$$\begin{aligned} Y = {} & 3.48 + 1.27A - 1.01\times10^{-3}B - 117.37C \\ & - 886.37D + 7.73\times10^{-5}A\times B - 0.03A\times C \\ & - 76.15A\times D + 2.59\times10^{-4}B\times C - 0.08B\times D \\ & + 428.46C\times D - 0.09A^2 + 7.98\times10^{-7}B^2 \\ & - 38.25C^2 + 16623.44D^2 \end{aligned} \quad (4)$$

3.2.2. Interactive effect of initial pH and conductivity value

Fig. 6 illustrates the interaction effect of initial pH and conductivity value on the decolorization rate of ATBA. The input power is 84 W and the CuO/AC dosage is 0.02 g. As could be seen from Fig. 6, the highest decolorization rate occurs when initial pH and conductivity value are minimum (2 and 100 μS/cm, respectively). Boguslavsky et al. [32] reported that about 10% energy was consumed in the transition layer after discharge, more energy was consumed for heating when the conductivity got higher, so the decolorization rate was reduced. In the process of DBD plasma discharge, ·OH can be produced. OH has stronger oxidation capacity under acidic conditions, leading to the increase of decolorization rate [33]. The decolorization rate is improved obviously when pH decreases, indicating that the effect of initial pH on the decolorization rate of ATBA is far greater than the initial conductivity.

Table 2
Experimental design and the corresponding results

Std. number	Initial pH	Conductivity value (μS/cm)	Input power (W)	CuO/AC dosage (g)	Decolorization rate (%)
1	7	100	84	0.00	87.97
2	7	2,500	63	0.02	66.33
3	12	2,500	84	0.02	79.32
4	7	2,500	84	0.04	80.78
5	7	1,300	63	0.00	77.30
6	7	2,500	105	0.02	90.00
7	7	1,300	84	0.02	81.63
8	2	1,300	63	0.02	74.52
9	7	100	63	0.02	67.58
10	12	1,300	63	0.02	58.02
11	12	100	84	0.02	75.36
12	2	100	84	0.02	84.07
13	7	1,300	63	0.04	67.60
14	2	1,300	84	0.04	88.64
15	12	1,300	84	0.04	59.88
16	7	100	84	0.04	82.68
17	7	1,300	84	0.02	87.00
18	12	1,300	105	0.02	75.94
19	2	1,300	84	0.00	93.88
20	2	2,500	84	0.02	86.18
21	7	100	105	0.02	90.87
22	7	1,300	84	0.02	82.58
23	7	1,300	84	0.02	79.03
24	7	1,300	105	0.04	91.59
25	7	1,300	84	0.02	81.28
26	7	1,300	105	0.00	93.59
27	2	1,300	105	0.02	92.63
28	12	1,300	84	0.00	87.97
29	7	2,500	84	0.00	91.56

3.2.3. Interactive effect of initial pH and input power

Fig. 7 reflects the interaction effect of initial pH and input power on the decolorization rate of ATBA. The conductivity value is 1,300 μS/cm and the Cu/AC dosage is 0.02 g. As shown in Fig. 7(a), response surface is steep, illustrating that the effects of pH value and input power on the decolorization rate of ATBA are both obvious. When the input power is the maximum and pH is the minimum (105 W and 2, respectively), the decolorization rate reaches to the highest value. The electrons get more energy under high interior input power. And it is beneficial to produce more active substances and high-energy electrons which could accelerate the degradation of ATBA [34], thus higher decolorization rate is obtained.

3.2.4. Interactive effect of initial pH and CuO/AC dosage

The interactive effect of initial pH and CuO/AC dosage on the decolorization rate of ATBA is shown in Fig. 8. The conductivity value is 1,300 μS/cm and the input power is 84 W. An elliptical contour plot represents that the interaction between corresponding variables is remarkable [35]. From Fig. 8(b), it could be seen that initial pH and CuO/AC dosage have an obvious interaction on the decolorization rate of ATBA. High decolorization rate occurs when the initial pH is minimum and the CuO/AC dosage is maximum (2 and 0.04 g, respectively) or the initial pH is about 5 without CuO/AC. Maybe it is owing to that the nature, ionization, and dissociation of the catalyst molecule was affected by the pH [36]. When the initial pH is too low, there are a large number of free ions in solution. The free ions are adsorbed to the surface of CuO/AC, which reduces the adsorption capacity of CuO/AC [37]. Therefore, CuO/AC dosage should be appropriately increased to get higher decolorization rate when the initial pH is 2.

3.2.5. Interactive effect of conductivity value and input power

Fig. 9 presents the effect of conductivity value and input power on the decolorization rate of ATBA when

Table 3
Analysis of variance

Source	Sum of squares	d*f*	Mean square	*F*-value	*p*-value Prob > *F*	
Model	2,567.83	14	183.42	12.74	<0.0001	Significant
A	580.07	1	580.07	40.3	<0.0001	
B	2.65	1	2.65	0.18	0.6738	
C	1,266.84	1	1,266.84	88.02	<0.0001	
D	311.09	1	311.09	21.61	0.0003	
AB	0.86	1	0.86	0.06	0.8102	
AC	9.29E-03	1	9.29E-03	6.46E-04	0.9801	
AD	130.49	1	130.49	9.07	0.0088	
BC	0.035	1	0.035	2.42E-03	0.9614	
BD	7.53	1	7.53	0.52	0.4807	
CD	14.87	1	14.87	1.03	0.3255	
A^2	31.25	1	31.25	2.17	0.1613	
B^2	9.06	1	9.06	0.63	0.4400	
C^2	81.27	1	81.27	5.65	0.0312	
D^2	95.93	1	95.93	6.67	0.0208	
Residual	215.89	15	14.39			
Lack of fit	154.43	10	15.44	1.26	0.4234	Not significant
Pure error	61.46	5	12.29			
Corrected total	2,783.72	29				

$R^2 = 0.9224$ and $R_{adj}^2 = 0.8501$.

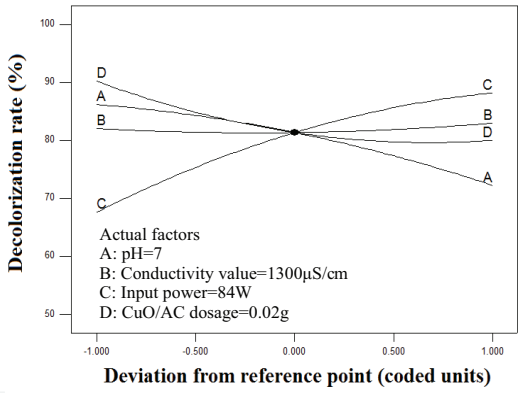

Fig. 5. Perturbation plot for decolorization rate.

initial pH is 7 and CuO/AC dosage is 0.02 g. From Table 3, the *p*-value of these two factors is 0.9614 (>0.05), showing that the interactive effect of conductivity value and input power on the degradation of ATBA is not obvious. As could be seen from Fig. 9(b), when the input power is kept constant, the decolorization rate of ATBA is basically unchanged although the conductivity value varies from 100 to 2,500 μS/cm. Therefore, the input power has a more sensitive effect on decolorization rate of ATBA compared with the conductivity value.

3.2.6. Interactive effect of conductivity value and CuO/AC dosage

Fig. 10 displays the interactive effect of conductivity value and CuO/AC dosage on the decolorization rate of ATBA at initial pH value of 7 and input power of 84 W. As the CuO/AC dosage increases gradually, the decolorization rate of ATBA increases first and then decreases. When the plasma reactor is combined with CuO/AC, better performance of plasma reactor can be achieved [16]. But at high catalyst dosage, the availability of surface active sites might decrease due to the aggregation of copper particle [38]. So the decolorization rate of ATBA decreases when the CuO/AC dosage is high. The *p*-value of conductivity and CuO/AC dosage is 0.4807 which is more than 0.05, indicating that the interactive effect between two factors on the decolorization rate of ATBA is not obvious.

3.2.7. Interactive effect of input power and CuO/AC dosage

As shown in Fig. 11, it mainly reflects the effect of input power and CuO/AC dosage on the decolorization rate of ATBA. The initial pH is 7 and conductivity value is 1,300 μS/cm. The input power and CuO/AC dosage both have great influences on the decolorization rate of ATBA. The decolorization rate of ATBA improves and then reduces as the CuO/AC dosage raises. With the increase of input power, the catalytic effect of CuO/AC is enhanced. It is mainly because that the energy injected into system is improved when input power increases. The generation rate of electron hole on the CuO/AC is accelerated, thus more active substances are produced in the reaction, resulting in the increase of decolorization rate [39].

3.2.8. Optimization and verification of the model

Through the response surface optimization analysis, the optimal degradation condition of ATBA is obtained.

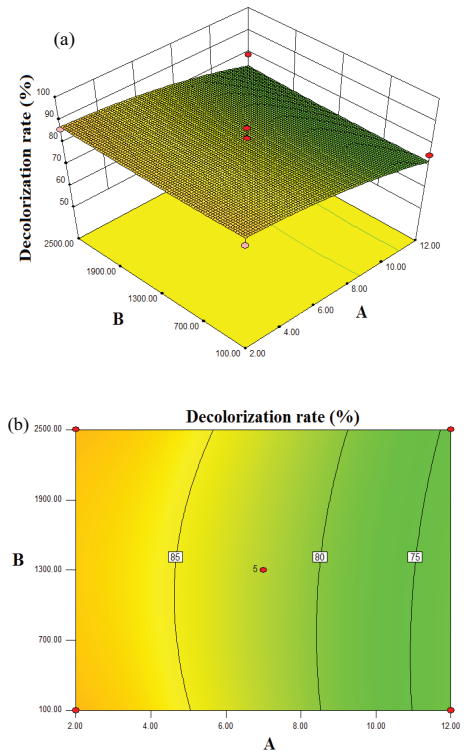

Fig. 6. Combined effects of initial pH (*A*) and conductivity value (*B*) on the decolorization rate (%): (a) response surface and (b) contour plot.

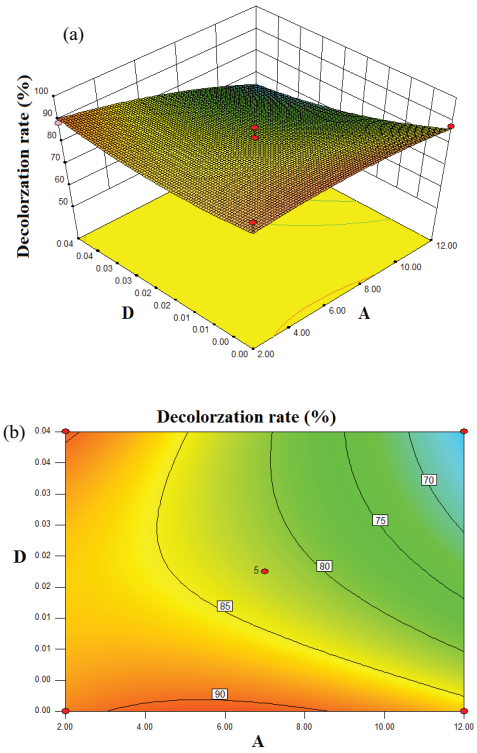

Fig. 8. Combined effects of initial pH (*A*) and CuO/AC dosage (*D*) on the decolorization rate (%): (a) response surface and (b) contour plot.

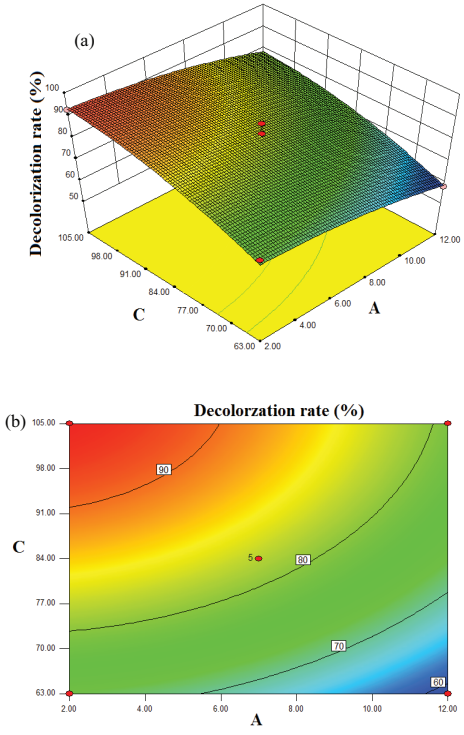

Fig. 7. Combined effects of initial pH (*A*) and input power (*C*) on the decolorization rate (%): (a) response surface and (b) contour plot.

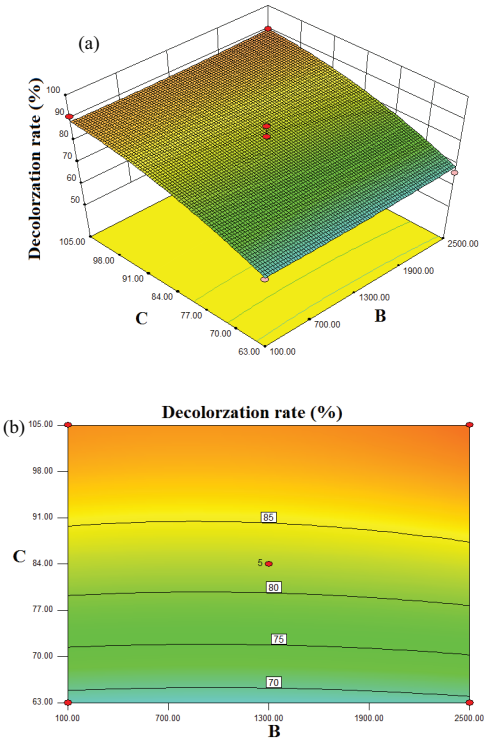

Fig. 9. Combined effects of conductivity value (*B*) and input power (*C*) on the decolorization rate (%): (a) response surface and (b) contour plot.

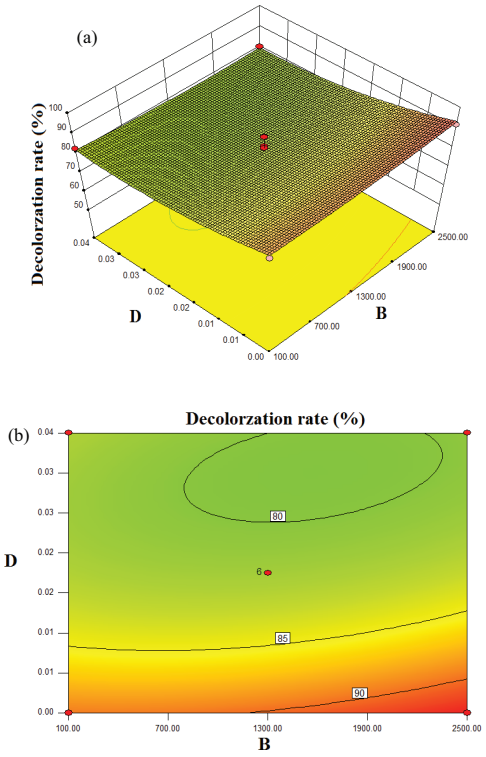

Fig. 10. Combined effects of conductivity value (*B*) and CuO/AC dosage (*D*) on the decolorization rate (%): (a) response surface and (b) contour plot.

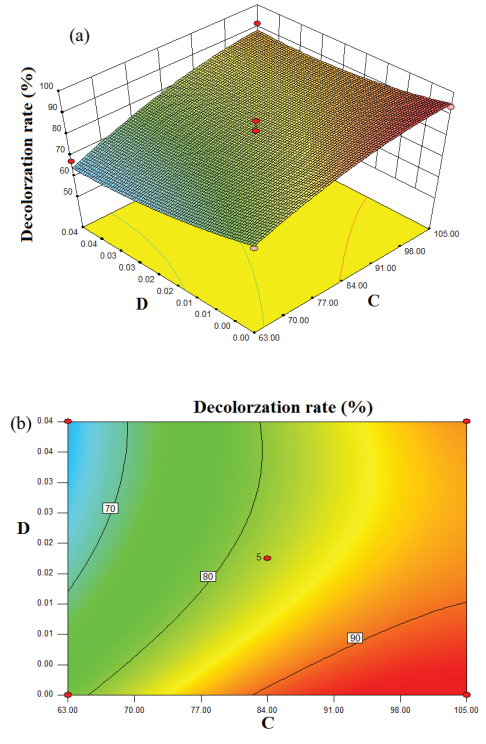

Fig. 11. Combined effects of input power (*C*) and CuO/AC dosage (*D*) on the decolorization rate (%): (a) response surface and (b) contour plot.

When initial pH is 2.64, conductivity value is 708.95 μS/cm, CuO/AC dosage is 0.03 g, and input power is 102.9 W, the predicted decolorization rate of ATBA reaches to 97.12%. Three parallel verification experiments are carried out under the optimal condition, and the experimental decolorization rate of ATBA is 95.87%. It can be seen that the experimental result matches the predicted value well. The relative error between predicted and experimental value is only 1.95%, which illustrates that the model is certain stable [40].

3.3. Synergistic effect of combined DBD plasma and CuO/AC system

Fig. 12 shows the decolorization rate and ultraviolet-visible (UV–Vis) absorption spectra by DBD plasma alone and DBD plasma coupled CuO/AC system. From Fig. 12(a), the synergistic effect of combined DBD plasma and CuO/AC is obvious. The decolorization rate of ATBA is significantly improved after applying CuO/AC to DBD plasma. As can be seen from Fig. 12(b), ATBA has three characteristic peaks at 311, 410, and 638 nm. The absorption peak at 638 nm represents the maximum absorption

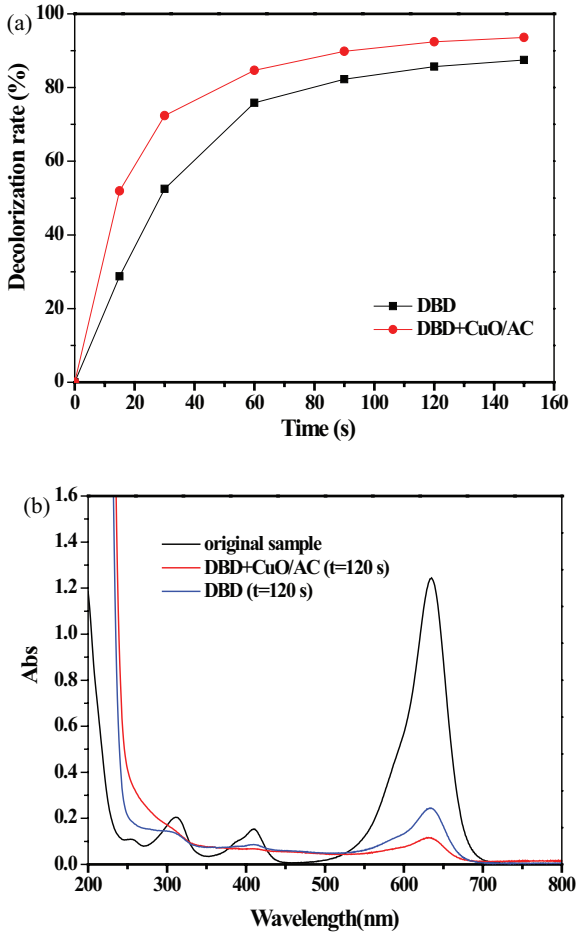

Fig. 12. Comparison of decolorization rate (a) and UV–Vis absorption spectra (b) under different systems, c_0 = 30 mg/L with original pH and conductivity, input power = 84 W, CuO/AC dosage = 0.2 g.

wavelength of ATBA. The absorption peaks at 311 and 410 nm represent aromatic compounds and conjugate system of carbonyl group and benzene ring, respectively. The characteristic absorption peaks are gradually disappeared and the popper becomes smooth after degradation, illustrating that the chemical bonds are disconnected and the dye molecules are degraded. Moreover, the popper of combined system becomes smoother than DBD plasma alone, indicating that combined DBD plasma and CuO/AC system has a synergistic effect.

3.4. Coupling mechanism

The possible coupling mechanism is proposed based on the above results (Fig. 13). During the discharge process, DBD plasma generator could stimulate high electric field and intense UV radiation [25]. In this atmosphere, electrons will be excited from the valence band of semiconductor to the conduction band. Therefore, CuO as a semiconductor could consequently produce the electron/hole pair [41]. The electron will capture O_2 into H_2O_2, and the hole can react with water or OH^- to generate a large amount of ·OH which could effectively destroy pollutant molecules. Moreover, other active species (O_3, $\cdot HO_2$, etc.) can be produced by DBD plasma generator. The relative equations are as follows [42,43]:

$$O_2 + e \rightarrow O_2^- \quad (5)$$

$$H_2O + e \rightarrow \cdot OH + \cdot H + e \quad (6)$$

$$O_2^- + \cdot H \rightarrow HO_2^- \quad (7)$$

$$HO_2^- + H^+ \rightarrow H_2O_2 \quad (8)$$

$$H_2O_2 + h\nu \rightarrow \cdot OH \quad (9)$$

$$O_{2(gas)} \rightarrow O_{3(gas)} \rightarrow O_{3(aq)} \quad (10)$$

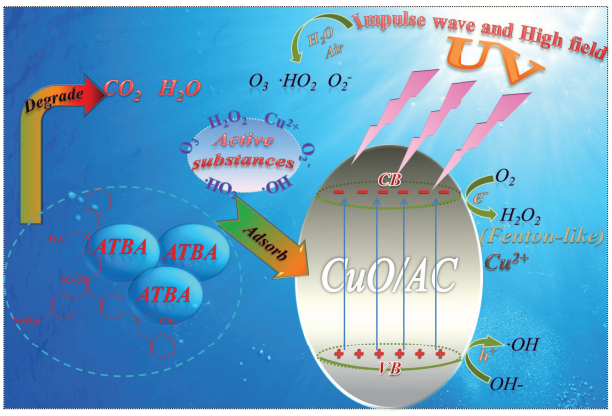

Fig. 13. Possible coupling mechanism of combined DBD plasma and CuO/AC.

What is more, a Fenton-like process could appear in the coupling system, the conduction-band electrons could reduce Cu(II) of CuO to Cu(I). And the Cu(I) presented in a catalyst structure will react with H_2O_2 to produce ·OH [41].

In the coupling system, CuO/AC acts not only as a catalyst, but also the adsorbent. SEM result shows that the prepared CuO/AC possesses a porous surface. Accordingly, dye molecules and active substances can be adsorbed over CuO/AC. And it contributes to the centralized degrading of dye molecules. Nekouei et al. [29] concluded that the protonation of functional group of CuO/AC can further enhance the adsorption of dye over CuO/AC particularly in highly acid solution, which is consistent with the RSM experimental result in this paper. The combination of adsorption by CuO/AC and catalytic oxidation by CuO results in higher decolorization rate of dye pollutant [44].

4. Conclusion

Combined DBD plasma and CuO/AC system can effectively degrade ATBA. The possible coupling mechanism of combined system is proposed. CuO/AC can be successfully prepared by the incipient wetness impregnation method at low temperature. Cu is loaded on AC in the form of CuO. The specific surface area and pore size distribution of CuO/AC are significantly changed compared with AC. The results of RSM present that influence sequence of single factor on decolorization rate is input power > initial pH > CuO/AC dosage > conductivity value, and the decolorization rate of ATBA reaches to 95.87% under optimal condition.

Acknowledgment

The authors would like to thank the financial support from National Natural Science Foundation of China (No. 21246010).

References

[1] L. Saikia, D. Bhuyan, M. Saikia, B. Malakar, D. K. Dutta, P. Sengupta, Photocatalytic performance of ZnO nanomaterials for self sensitized degradation of malachite green dye under solar light, Appl. Catal., A, 490 (2015) 42–49.
[2] W.H. Li, Q.Y. Yue, B.Y. Gao, Z.H. Ma, Y.J. Li, H.X. Zhao, Preparation and utilization of sludge-based activated carbon for the adsorption of dyes from aqueous solutions, Chem. Eng. J., 171 (2011) 320–327.
[3] H. Qiao, Y.M. Zhou, F. Yu, E. Wang, Y.H. Min, Q. Huang, L.F. Pang, T.S. Ma, Effective removal of cationic dyes using carboxylate-functionalized cellulose nanocrystals, Chemosphere, 141 (2015) 297–303.
[4] C. Gaidau, M.D. Niculescu, L. Surdu, L. Dinca, I. Barbu, Improved properties of wool on sheepskins by low pressure plasma treatment, Ind. Textila, 68 (2017) 193–196.
[5] A. Haji, S.S. Qavamnia, F.K. Bizhaem, Optimization of oxygen plasma treatment to improve the dyeing of wool with grape leaves, Ind. Textila, 67 (2016) 244–249.
[6] A. Haji, M. Khajeh Mehrizi, J. Sharifzadeh, Dyeing of wool with aqueous extract of cotton pods improved by plasma treatment and chitosan: optimization using response surface methodology, Fibers Polym., 17 (2016) 1480–1488.
[7] A. Haji, S.S. Qavamnia, Response surface methodology optimized dyeing of wool with cumin seeds extract improved with plasma treatment, Fibers Polym., 16 (2015) 46–53.
[8] T. Zadi, A.A. Assadi, N. Nasrallah, R. Bouallouche, P.N. Tri, A. Bouzaza, M.M. Azizi, R. Maachi, D. Wolbert, Treatment of

hospital indoor air by a hybrid system of combined plasma with photocatalysis: case of trichloromethane, Chem. Eng. J., 349 (2018) 276–286.
[9] A.A. Assadi, S. Loganathan, P.N. Tri, S. Gharib-Abou Ghaida, A. Bouzaza, A.N. Tuan, D. Wolbert, Pilot scale degradation of mono and multi volatile organic compounds by surface discharge plasma/TiO_2 reactor: investigation of competition and synergism, J. Hazard. Mater., 357 (2018) 305–313.
[10] C.A. Aggelopoulos, D. Tataraki, G. Rassias, Degradation of atrazine in soil by dielectric barrier discharge plasma-Potential singlet oxygen mediation, Chem. Eng. J., 347 (2018) 682–694.
[11] H. Fan, G.Y. Yao, W. Liu, Z.H. Xing, J.M. Shi, B. Gao, Y. Chen, Experimental study on the treatment of mercury contained soil by thermal analytical low temperature plasma based on cold atomic absorption spectrophotometry, Spectrosc. Spect. Anal., 38 (2018) 2279–2283.
[12] S. Zhao, C.j. Hao, D. Xu, Y.Y. Wen, J. Qiu, K.F. Liu, Effect of electrical parameters on energy yield of organic pollutant degradation in a dielectric Barrier discharge reactor, IEEE Trans. Plasma Sci., 45 (2017) 1043–1050.
[13] Y.J. Shen, Q.H. Xu, Y.W. Pan, J.D. Ding, Y. Wang, Kinetics of the ozone oxidation of weak acid brilliant green in aqueous solution, Fresen. Environ. Bull., 25 (2016) 2554–2562.
[14] A. Mercado-Cabrera, B. Jaramillo-Sierra, R. Pena-Eguiluz, R. Lopez-Callejas, B.G. Rodriguez-Mendez, R. Valencia-Alvarado, A.N. Hernandez-Arias, A.E. Munoz-Castro, Simultaneous degradation of toxic organic pollutants by thin-falling-water-film DBD reactor, Desal. Wat. Treat., 101 (2018) 157–169.
[15] H. Zhang, Q.F. Zhang, C.G. Miao, Q. Huang, Degradation of 2, 4-dichlorophenol in aqueous solution by dielectric barrier discharge: effects of plasma-working gases, degradation pathways and toxicity assessment, Chemosphere, 204 (2018) 351–358.
[16] C. He, L. Cao, X. Liu, W. Fu, J. Zhao, Catalytic behavior and synergistic effect of nonthermal plasma and CuO/AC catalyst for benzene destruction, Int. J. Environ. Sci. Technol., 12 (2015) 3531–3540.
[17] J. Chen, H. Pan, H.J. Hou, H.B. Li, J.K. Yang, L.L. Wang, High efficient catalytic degradation of PNP over Cu-bearing catalysts with microwave irradiation, Chem. Eng. J., 323 (2017) 444–454.
[18] H.H. Tseng, M.Y. Wey, Y.S. Liang, K.H. Chen, Catalytic removal of SO_2, NO and HCl from incineration flue gas over activated carbon-supported metal oxides, Carbon, 41 (2003) 1079–1085.
[19] Z. Zhang, X.B. Ma, P.B. Zhang, Y.M. Li, S.P. Wang, Effect of treatment temperature on the crystal structure of activated carbon supported $CuCl_2$-$PdCl_2$ catalysts in the oxidative carbonylation of ethanol to diethyl carbonate, J. Mol. Catal. A, 266 (2007) 202–206.
[20] O.S. Chan, W.H. Cheung, G. McKay, Single and multicomponent acid dye adsorption equilibrium studies on tyre demineralised activated carbon, Chem. Eng. J., 191 (2012) 162–170.
[21] Y.E. Unsal, M. Soylak, M. Tuzen, Column solid-phase extraction of sunset yellow and spectrophotometric determination of its use in powdered beverage and confectionery products, Int. J. Food Sci. Technol., 47 (2012) 1253–1258.
[22] M. Berrios, M.A. Martin, A. Martin, Treatment of pollutants in wastewater: adsorption of methylene blue onto olive-based activated carbon, J. Ind. Eng. Chem., 18 (2012) 780–784.
[23] Z.D. Ren, S.S. Quan, Y.C. Zhu, L. Chen, W.X. Deng, B.A. Zhang, Purification of yellow phosphorus tail gas for the removal of PH_3 on the spot with flower-shaped CuO/AC, RSC Adv., 5 (2015) 29734–29740.
[24] S.S. Moghaddam, M.R.A. Moghaddam, M. Arami, Response surface optimization of acid red 119 dye from simulated wastewater using Al based waterworks sludge and polyaluminium chloride as coagulant, J. Environ. Manage., 92 (2011) 1284–1291.
[25] H.Y. Fu, P.C. Xu, G.H. Huang, T. Chai, M. Hou, P.F. Gao, Effects of aeration parameters on effluent quality and membrane fouling in a submerged membrane bioreactor using Box-Behnken response surface methodology, Desalination, 302 (2012) 33–42.
[26] X.W. Zhang, M.H. Zhou, L. Lei, Preparation of photocatalytic TiO_2 coatings of nanosized particles on activated carbon by AP-MOCVD, Carbon, 43 (2005) 1700–1708.
[27] N.R. Chen, Q.J. Lin, Q.Z. Zeng, J.P. Rao, Optimization of preparation conditions of soy flour adhesive for plywood by response surface methodology, Ind. Crop. Prod., 51 (2013) 267–273.
[28] Z. Abbasi, M. Haghighi, E. Fatehifar, S. Saedy, Synthesis and physicochemical characterizations of nanostructured Pt/Al_2O_3-CeO_2 catalysts for total oxidation of VOCs, J. Hazard. Mater., 186 (2011) 1445–1454.
[29] F. Nekouei, S. Nekouei, I. Tyagi, V.K. Gupta, Kinetic, thermodynamic and isotherm studies for acid blue 129 removal from liquids using copper oxide nanoparticle-modified activated carbon as a novel adsorbent, J. Mol. Liq., 201 (2015) 124–133.
[30] B.K. Korbahti, M.A. Rauf, Response surface methodology (RSM) analysis of photoinduced decoloration of toludine blue, Chem. Eng. J., 136 (2008) 25–30.
[31] A. Haji, S.S. Qavamnia, M. Nasiriboroumand, The use of D-optimal design in optimization of wool dyeing with Juglans regia bark, Ind. Textila, 69 (2018) 104–110.
[32] L.Z. Boguslavsky, S.A. Khainatsky, A.N. Shcherbak, Optical studies of the plasma-liquid transition layer in pulsed corona discharges in strong water electrolytes, Tech. Phys., 46 (2001) 174–178.
[33] J.Z. Gao, L.M. Pu, W. Yang, J. Yu, Y. Li, Oxidative degradation of nitrophenols in aqueous induced by plasma with submersed glow discharge electrolysis, Plasma Process. Polym., 1 (2004) 171–176.
[34] J. Gao, P.D. Gu, L. Yuan, F.C. Zhong, Degradation of dye wastewater by ns-pulse DBD plasma, Plasma Sci. Technol., 15 (2013) 928–934.
[35] H.L. Liu, Y.R. Chiou, Optimal decolorization efficiency of Reactive Red 239 by UV/TiO_2 photocatalytic process coupled with response surface methodology, Chem. Eng. J., 112 (2005) 173–179.
[36] Q. Darugar, W. Qian, M.A. El-Sayed, M.P. Pileni, Size-dependent ultrafast electronic energy relaxation and enhanced fluorescence of copper nanoparticles, J. Phys. Chem. B, 110 (2006) 143–149.
[37] M. Ghaedi, F. Karimi, B. Barazesh, R. Sahraei, A. Daneshfar, Removal of Reactive Orange 12 from aqueous solutions by adsorption on tin sulfide nanoparticle loaded on activated carbon, J. Ind. Eng. Chem., 19 (2013) 756–763.
[38] N.N. Fathima, R. Aravindhan, J.R. Rao, B.U. Nair, Dye house wastewater treatment through advanced oxidation process using Cu-exchanged Y zeolite: a heterogeneous catalytic approach, Chemosphere, 70 (2007) 1146–1151.
[39] K.F. Shang, X.J. Wang, J. Li, H. Wang, N. Lu, N. Jiang, Y. Wu, Synergetic degradation of Acid Orange 7 (AO7) dye by DBD plasma and persulfate, Chem. Eng. J., 311 (2017) 378–384.
[40] Y.J. Shen, Q.H. Xu, J.M. Shi, M. Li, Y. Zhang, Optimization and mechanism study of C.I. Acid Blue 25 wastewater degradation by ozone/Fenton oxidation process: response surface methodology, intermediate products and degradation pathway, Desal. Wat. Treat., 65 (2017) 313–326.
[41] A.P.L. Batista, H.W.P. Carvalho, G.H.P. Luz, P.F.Q. Martins, M. Goncalves, L.C.A. Oliveira, Preparation of CuO/SiO_2 and photocatalytic activity by degradation of methylene blue, Environ. Chem. Lett., 8 (2010) 63–67.
[42] Y. Li, R.J. Yi, C.W. Yi, B.Y. Zhou, H.J. Wang, Research on the degradation mechanism of pyridine in drinking water by dielectric barrier discharge, J. Environ. Sci. China, 53 (2017) 238–247.
[43] Y. Sun, Y.A. Liu, R. Li, X. Li, H. Chen, G. Xue, S. Ognier, Reactive blue degradation in aqueous medium by Fe-doping TiO_2 catalytic nonthermal plasma, IEEE Trans. Plasma Sci., 43 (2015) 3234–3241.
[44] B. Zhao, H.H. Yi, X.L. Tang, Q. Li, D.D. Liu, F.Y. Gao, Copper modified activated coke for mercury removal from coal-fired flue gas, Chem. Eng. J., 286 (2016) 585–593.